tvst

DOI: 10.1167/tvst.6.3.17

Article

Long-Term Efficacy of GMP Grade Xeno-Free hESC-Derived RPE Cells Following Transplantation

Trevor J. McGill[1,2], Osnat Bohana-Kashtan[3], Jonathan W. Stoddard[2], Michael D. Andrews[1], Neelay Pandit[1], Lior R. Rosenberg-Belmaker[3], Ofer Wiser[3], Limor Matzrafi[3], Eyal Banin[4], Benjamin Reubinoff[5,6], Nir Netzer[3], and Charles Irving[3]

[1] Casey Eye Institute, Oregon Health & Science University (OHSU), Portland, OR, USA
[2] Department of Neuroscience, Oregon National Primate Research Center, OHSU, Beaverton, OR, USA
[3] Cell Cure Neurosciences Ltd., Jerusalem, Israel
[4] Center for Retinal and Macular Degenerations, Department of Ophthalmology, Hadassah-Hebrew University Medical Center, Jerusalem, Israel
[5] The Goldyne Savad Institute of Gene Therapy, Sidney and Judy Swartz Embryonic Stem Cell Research Center, Hadassah-Hebrew University Medical Center, Jerusalem, Israel
[6] The Department of Obstetrics and Gynecology, Hadassah-Hebrew University Medical Center, Jerusalem, Israel

Correspondence: Trevor J. McGill, PhD, Casey Eye Institute, OHSU, 3375 SW Terwilliger Blvd., Portland, OR 97239, USA. e-mail: mcgilltr@ohsu.edu

Received: 21 January 2017
Accepted: 14 April 2017
Published: 14 June 2017

Keywords: RPE cells; transplantation; AMD; Xeno-free

Citation: McGill TJ, Bohana-Kashtan O, Stoddard JW, Andrews MD, Pandit N, Rosenberg-Belmaker LA, Wiser O, Matzrafi L, Banin E, Reubinoff B, Netzer N, Irving C. Long-term efficacy of GMP grade xeno-free hESC-derived RPE cells following transplantation. Trans Vis Sci Tech. 2017; 6(3):17, doi:10.1167/tvst.6.3.17

Purpose: Retinal pigment epithelium (RPE) dysfunction underlies the retinal degenerative process in age-related macular degeneration (AMD), and thus RPE cell replacement provides an optimal treatment target. We characterized longitudinally the efficacy of RPE cells derived under xeno-free conditions from clinical and xeno-free grade human embryonic stem cells (OpRegen) following transplantation into the subretinal space of Royal College of Surgeons (RCS) rats.

Methods: Postnatal (P) day 20 to 25 RCS rats ($n = 242$) received a single subretinal injection of 25,000 (low)-, 100,000 (mid)-, or 200,000 (high)-dose xeno-free RPE cells. BSS+ (balanced salt solution) (vehicle) and unoperated eyes served as controls. Optomotor tracking (OKT) behavior was used to quantify functional efficacy. Histology and immunohistochemistry were used to evaluate photoreceptor rescue and transplanted cell survival at 60, 100, 150, and 200 days of age.

Results: OKT was rescued in a dose-dependent manner. Outer nuclear layer (ONL) was significantly thicker in cell-treated eyes than controls up to P150. Transplanted RPE cells were identified in both the subretinal space and integrated into the host RPE monolayer in animals of all age groups, and often contained internalized photoreceptor outer segments. No pathology was observed.

Conclusions: OpRegen RPE cells survived, rescued visual function, preserved rod and cone photoreceptors long-term in the RCS rat. Thus, these data support the use of OpRegen RPE cells for the treatment of human RPE cell disorders including AMD.

Translational Relevance: Our novel xeno-free RPE cells minimize concerns of animal derived contaminants while providing a promising prospective therapy to the diseased retina.

Introduction

Age-related macular degeneration (AMD) is the most prevalent cause of irreversible visual disability and blindness in the elderly in the developed world. AMD is estimated to affect 10 million older individuals in the United States alone, including 2 million with advanced AMD,[1,2] a number projected to increase to 5.5 million by 2050. Early to intermediate stages of AMD, often referred to as "dry AMD," are characterized by the progressive accumulations of deposits of proteins and extracellular debris known as drusen beneath the retinal pigment epithelial (RPE) cells. The progressive accumulation of drusen in the macula is correlated with progression to more advanced forms of AMD.

There are two primary forms of advanced AMD. The exudative or "wet" form, which accounts for approximately15% of total AMD cases[1,3,4] and is characterized by subretinal choroidal neovascularization resulting in fragile and leaky blood vessels that penetrate through Bruch's membrane and cause bleeding, edema, and scar tissue formation resulting in acute retinal cell loss and severe loss of vision. The nonexudative form of advanced AMD, termed geographic atrophy (GA), and is characterized by the progressive death of RPE cells followed by the subsequent death of the apposed photoreceptors. Death of photoreceptors in the macula results in progressive and expanding impaired central vision.

Treatments for AMD are limited. Exudative AMD can be controlled relatively well with intraocular injections of anti-VEGF therapies, however, there are no approved therapies for GA. Dietary supplements of antioxidant vitamins and minerals and increased intake of macular carotenoids are recommended[5] and may be beneficial[6]; however, these dietary supplements only reduce the risk of progression to advanced AMD, are only effective in a relatively small proportion of patients, and are likely to be less effective with increasing advancement of GA. Other experimental therapies for AMD exist, including small molecule therapy,[7] treatments using growth factors,[8–14] and cell transplantation,[15–17] and many of these approaches are currently being examined in Food and Drug Administration (FDA)-approved clinical trials. In addition, multiple cell-based therapy clinical trials have begun phase I/II, primarily designed to examine the safety of cell transplantation in late-stage AMD.[18–20] While multiple approaches to treating AMD may be efficacious, cell transplantation offers significant advantages over other methods as it includes a highly biologically relevant approach of directly replacing the degenerated cell type(s) and holds the potential for a single therapeutic treatment to provide long-term efficacy that could last years or perhaps even decades.

The optimal cell-based therapy strategy currently is to prevent photoreceptor and subsequent vision loss through the delivery of therapeutic cells at an early stage of disease, prior to significant photoreceptor cell death and disease progression. A number of experimental studies have used this approach in the Royal College of Surgeons (RCS) rat model. The RCS rat expresses a mutation in the Mertk gene[21] that results in severely impaired ability of the host RPE cells to phagocytose shed photoreceptor outer segments.[22,23] As a result, a toxic debris zone accumulates and results in the progressive death of photoreceptors and subsequent vision loss.[16,24,25] Thus, the RCS rat serves as a model of retinal degenerative disease (RDD), in which, a primary dysfunction within the RPE cells results in secondary photoreceptor loss and visual impairment, akin to disease progression in AMD. Transplantation of potentially therapeutic cells into the subretinal space of the RCS rat has been demonstrated to rescue rod and cone photoreceptors, maintain electrophysiological responses including electroretinogram and cellular recordings from the superior colliculus, and minimize the deterioration of behaviorally measured spatial vision.[16,24,26,27] While various cell types have been used to demonstrate efficacy in the RCS rat, transplantation of RPE cells remains of particular interest as a means to prevent or to replace the loss of host RPE cells that precedes photoreceptor loss in AMD. Indeed, transplantation of RPE cells into the RCS rat has been shown to be effective.[17,27–39]

As a result of the large body of RPE cell transplantation preclinical studies, multiple early phase clinical trials for macular degenerating diseases have begun. In phase 1/2 studies conducted in the United States and Europe, using human embryonic stem cells (hESCs)-derived RPE cells formulated as cell suspension have been injected into the subretinal space of AMD and Stargardt's macular dystrophy patients. A recent report described that the treatments were well tolerated and safe.[19,20] Other approaches in preclinical studies have used a RPE cell monolayer, either with or without a scaffold, with the intent of implantation under the area where degenerating photoreceptors were present but host RPE have died.[18,28] Using this approach, implantation of a 1.3 × 3.0-mm sheet of induced pluripotent stem cells (iPSCs)-derived RPE cells were recently transplanted into an eye of an AMD patient.[40] Ultimately, a number of approaches are currently being explored for RPE cell based therapy, both preclinical and in early Phase 1/2 clinical trials.

A significant regulatory safety concern regarding translation of preclinical cell transplantation studies into human clinical trials is to ensure the cell product is free from potentially harmful material. As many protocols for generation of RPE cells require products from other species, the presence of potentially harmful agents of animal origin, such as prions, continues to be of concern. To eliminate potentially harmful cross species material, we have developed an RPE cell line (OpRegen, Cell Cure Neurosciences Ltd., Jerusalem, Israel) using a directed differentia-

tion protocol from hESCs, using a strict and completely xeno-free (animal product–free)-derived reagents protocol. To evaluate potential therapeutic efficacy and adequacy for potential use in a clinical trial, we performed a longitudinal survival and efficacy study of OpRegen xeno-free RPE cells transplanted into the RCS rat.

Methods

Cells

OpRegen cell therapy product is a cryopreserved single cell suspension of RPE cells derived under xeno-free and Good Manufacturing Practice (GMP) conditions from clinical xeno-free GMP-grade hESCs (line HAD-C 102[41]) through a directed differentiation process with Nicotinamide (Sigma, St. Louis, MO) and Activin A (Peprotech, Rocky Hill, NJ).[42] Briefly, HAD-C 102 hESCs are expanded as colonies on irradiated xeno-free GMP-grade human umbilical cord fibroblast feeders (line CRD008). To initiate differentiation to RPE, collagenase A (Worthington, Lakewood, NJ) harvested hESCs are transferred to feeder-free Hydrocell plates (CellSeed, Tokyo, Japan) for 1 week of growth in the presence of 10-mM nicotinamide under low oxygen atmosphere (5%) conditions (37°C, 5% CO_2) for the generation of spheroid bodies (SBs). Week old SBs are then collected, dissociated gently by pipetting, and transferred to human laminin (Biolamina, Solna, Sweden)–coated plates for an additional week of growth under low oxygen atmosphere (5%) in the presence of 10-mM nicotinamide. Cells are then cultured under low oxygen (5%) atmosphere for an additional 3 to 4 weeks; 2 weeks in the presence 10-mM nicotinamide and 140-ng/mL Activin A, followed by 1 to 2 weeks in the presence of 10-mM nicotinamide only. When areas of light pigmentation become apparent in patches of polygonal cells, plates are transferred to normal oxygen (20%) atmosphere (37°C, 5% CO_2) for 1 to 2 weeks of growth in the presence of 10-mM nicotinamide. After 1 to 2 weeks, polygonal patches with distinctive pigmentation become apparent within areas of nonpigmented cells. Nonpigmented areas are manually removed with a sterile tip and the remaining pigmented cells are detached and collected using TrypLE Select (Invitrogen, City, State, Country). Pigmented cells (Passage 0) are then expanded on gelatin (Fibrogen, Carlsbad, CA)-coated culture plates, harvested at passage 2 and cryopreserved. OpRegen cells are then characterized for viability, purity, and identity (%CRALBP$^+$PMEL-17$^+$ double positive cells by FACS, %Bestrophin 1–positive and %MITF (microphthalmia-associated transcription factor)–positive cells by confocal microscopy and DNA fingerprinting), level of hESCs impurity (%Oct4$^+$TRA-1-60$^+$ cells by FACS [fluorescence-activated cell sorting]), morphology, functional activity (barrier function and polarized secretion of PEDF [pigment epithelium-derived factor] and VEGF [vascular endothelial growth factor]), karyotyping, and sterility (see Table 2 for antibody details).

OpRegen RPE cells were prepared in an identical manner for each transplantation. A frozen vial containing approximately 1.5 million cells was thawed at 37°C. The cells were centrifuged at 3000 rpm for 5 minutes. The supernatant was aspirated and the cell pellet was resuspended in 1.5 mL of human serum–containing medium. Cells were counted using a hemocytometer and cell viability determined using Trypan blue (Biological Industries, Beit Haemek, Israel). Following an additional round of centrifugation at 3000 rpm for 5 minutes, the supernatant media was aspirated and cell pellet was resuspended in 5 mL of sterile BSS+ (Alcon, Fort Worth, TX). To ensure adequate rinsing of media, cells were centrifuged again (3000 rpm for 5 minutes) and resuspended in 1 mL of sterile BSS+. Cells were then recounted and viability was determined. Using this final count, the remaining cells were centrifuged and distributed into aliquots containing concentrations of 12,500, 50,000, and 100,000 cells/μL. Cell viability was also determined at the conclusion of each transplantation session.

Animals

Pigmented RCS (RCS-p+/Lav) rats ($n = 242$) were used for this study. All animals were fed a standard laboratory chow and maintained on a 12-hour dark/light cycle. All animals were monitored daily for general health and ophthalmic condition. Animals were grouped according to survival ages (P) and sacrificed at 60, 100, 150, and 200 days postnatal (represented hereafter as P60, P100, P150, and P200). Each group contained five dosage groups: untreated, vehicle control BSS+, 25,000 (low), 100,000 (mid), or 200,000 (high) OpRegen cells (Table 1). Efforts were made to evenly distribute animals from each litter to each dosage, survival group, and sex in an attempt to avoid potential animal bias. All study animals were maintained on oral cyclosporine A (210 mg/L; Gengraf, North Chicago, IL) administered in drinking water from 1 day prior to surgery until sacrifice.[16]

Table 1. Summary Table of the Study Design

Treatment	Animals	Survival Groups P60	P100	P150	P200
Untreated	$N = 37$	$N = 11$ OKT Histology IHC	$N = 10$ OKT Histology IHC	$N = 9$ OKT Histology IHC	$N = 7$ OKT Histology IHC
Vehicle control BSS plus	$N = 46$	$N = 11$ OKT Histology IHC	$N = 8$ OKT Histology IHC	$N = 13$ OKT Histology IHC	$N = 14$ OKT Histology IHC
25,000 OpRegen cells (low dose)	$N = 49$	$N = 10$ OKT Histology IHC	$N = 12$ OKT Histology IHC	$N = 15$ OKT Histology IHC	$N = 12$ OKT Histology IHC
100,000 OpRegen cells (mid dose)	$N = 57$	$N = 13$ OKT Histology IHC	$N = 15$ OKT Histology IHC	$N = 17$ OKT Histology IHC	$N = 12$ OKT Histology IHC
200,000 OpRegen cells (high dose)	$N = 53$	$N = 15$ OKT Histology IHC	$N = 14$ OKT Histology IHC	$N = 13$ OKT Histology IHC	$N = 11$ OKT Histology IHC

RCS rats used for this study were grouped according to survival ages (P) sacrificed at 60, 100, 150, and 200 days of age. Each survival group contained five dosage groups: untreated, vehicle control BSS+, 25,000 cells (low dose), 100,000 cells (mid dose), or 200,000 cells (high dose). Number of animals (N), histology and efficacy assessments over the course of the study are listed (in abbreviated form) in the boxes that correspond to the cohort they were performed on. IHC, immunohistochemistry.

All animal procedures were conducted under the approval of the Institutional Animal Care and Use Committee (IACUC) at Oregon Health & Science University, which are in accordance with the ARVO Statement for the Use of Animals in Ophthalmic and Vision Research.

Transplantation

On P21 to P25, RCS rats were anesthetized with 2, 2, 2-Tribromoethanol (intraperitoneal; 230 mg/kg; Sigma) and eyes received topical 0.5% proparacaine HCl anesthesia. Pupils were dilated with 1% tropicamide and 2.5% phenylephrine HCl and the eye was slightly proptosed. A small scleral/choroidal incision (~1 mm) was made 2-mm posterior to the limbus in the dorsotemporal region using increasing gauge needle tips. A small lateral corneal puncture was made using a 30-G needle to limit increases of intraocular pressure and reduce efflux of cells following injection. Two microliters of suspension containing the total cell dose was delivered into the subretinal space of one eye using a fine glass pipette (internal diameter, 75–150 μm) inserted into the subretinal space. The glass pipette was connected to a 10-μL Hamilton syringe (Hamilton, Reno, NV) with small-bore (400-μL total volume) microtubing. The sclerotomy was then sutured closed using 9-0 polypropylene suture. The contralateral, noninjected, eye was left intact and used as an unoperated control. Successful surgery was confirmed by observation of a subretinal bleb through color fundus photography acquired immediately following surgery (Micron III Retinal Imaging Microscope; Phoenix Research Labs, Pleasonton, CA). All animals received injection of cells with a minimum cell viability of 90%. Only animals with successful subretinal injections were included in the study, and those without were removed. The animals were recovered from anesthesia and replaced in their home cage. All animals received daily intraperitoneal injections of dexamethasone (1.6

Table 2. Summary of Qualified Antibodies with Sources and Optimal Dilutions Used for Detecting OpRegen Implanted Subretinally into the Dystrophic RCS Rat Eye, and for OpRegen Characterization by FACS and Immunostaining

Primary Antibody	Source	Dilution
Anti-Melanoma gp100 (PMEL17) (FACS)	Clone EPR4864, Cat#AB137062; Abcam (Cambridge, MA)	1.4 ug/0.1 mL
Anti-CRALBP	Clone B2; Abcam	2 ug/0.1 mL
Anti-MITF	Clone D5; Thermo Scientific (Fremont, CA)	0.2 ug/0.1 mL
Anti-TRA-1-60 PE	Clone TRA-1-60; BD (San Diego, CA)	1:5 0.3ug/0.1 mL
Anti-Oct 3/4	Clone 050-808; BD	1:10 5ug/0.1 mL
Anti-ZO1	Invitrogen (Carlsbad, CA)	1:50
Anti-Bestrophin 1	Clone E6-6; Novus Biologicals (Littleton, CO)	1:100
Anti-Melanoma gp100 (PMEL17)	Clone EPR4864, Cat#AB137062; Abcam	1:500
Anti-Ki67	Clone EPR4864, Cat#AB137062; Abcam	1:500
Anti-Human Nuclear Marker	Clone 3E1.3, Cat#MAB4383; Millipore (Temecula, CA)	1:300
Anti-RPE65	Cat#ab105366; Abcam	1:250
Anti-Ki67	Clone EPR4864, Cat#AB137062; Abcam	1:500
Anti-Cone Arrestin	Cat#AB15282; Millipore	1:10,000
Anti-Rhodopsin	Clone Rho 1D4, Cat#MAB5356; Millipore	1:5000

mg/Kg) for 2 weeks post cell transplantation to minimize a potential inflammatory response.

Optokinetic Tracking

Optokinetic tracking (OKT) thresholds were measured and recorded in a masked fashion where the operator was unaware of to which group the animal being tested belonged. OKT thresholds were measured using a virtual optomotor system (VOS; CerebralMechanics, Lethbridge, Alberta, Canada) comprised of four computer monitors arranged in a square, displays facing inward. On the monitors, a virtual cylinder is generated displaying sine-wave gratings that can be rotated either clockwise or counter clockwise permitting evaluation of both the left and right eyes independently; the left eye only responds to clockwise, and the right eye only to counterclockwise movement.[25,43,44] Beginning with a low spatial frequency, the cylinder was rotated and if the grating is resolved, the animal would then respond with a reflexive head and neck movement tracking the grating. The spatial frequency of the grating was then incrementally increased until the rat no longer tracked the stimulus, resulting in a maximal spatial frequency threshold. Maximum spatial frequency thresholds were measured in all groups through both eyes independently at 60, 100, 150, and 200 days of age.

Histology and Immunohistochemistry

At P60, P100, P150, and P200, both eyes from each animal were harvested, fixed in 4% paraformaldehyde for approximately 1 hour, cryoprotected in increasing sucrose gradients, embedded in optimum cutting temperature compound, and frozen. Frozen blocks were cryosectioned at 12 μm. Sixty slides containing four sections per slide were obtained for each eye. Sections were collected in a five-slide series to provide a tissue section every 60 μm throughout the eye using only the first slide of every series (slide 1, 6, 11, etc.), which were then stained using cresyl violet acetate (Sigma). Cresyl violet–stained sections were examined for: (1) injection site and suture location, (2) photoreceptor rescue, (3) evidence of transplanted cells, and (4) untoward pathology such as tumors/uncontrolled cell growth or damage to the host retina not due to surgical manipulations. For each slide, the maximum outer nuclear (ONL) layer thickness was recorded for quantification of rescue. In addition, cresyl violet–stained slides from BSS+ and high dose cell–treated (200 K) eyes were sent for additional blinded safety review to an external veterinary pathologist.

OpRegen cell–treated eye slides selected for immunofluorescence (IF) were chosen from cresyl violet–stained sections that contained cells in the subretinal

space consistent with the size and morphology of the transplanted human cells and had significant protection of the host ONL. Sections of OpRegen cell–treated and untreated RCS rat retina, OpRegen cell pellets, human retina, human tonsil, and human melanoma were used to qualify the multiple antibodies used (Table 2). All IF staining (except for cone arrestin) was performed as double primary stains and 4′,6-diamidino-2-phenylindole (DAPI; Sigma) served as a background nuclear stain. At least one slide from each cell-treated animal was used for each staining run. Three primary antibody-staining runs were performed: #1- rabbit monoclonal anti-melanoma gp100 (PMEL17, Clone EPR4864; human specific, cat#ab137062; Abcam, Cambridge, MA) costained with mouse monoclonal anti-nuclei marker (HuNu, Clone 3E1.3, cat#MAB4383; Millipore, Temecula, CA) for detecting human RPE and any non-RPE human cells. Antibody run #2: rabbit monoclonal Anti-Ki67 (Ki67; Clone EPR3610, human specific, cat#ab92742; Abcam) and antinuclear marker for detecting proliferating human cells. Antibody run #3: rabbit polyclonal anti-rat cone arrestin (cat#ab15282; Millipore) to evaluate sections for cone counting. In addition, selected slides were stained using mouse monoclonal anti-rhodopsin (Clone Rho 1D4, MAB5356; Millipore) in combination with PMEL17 to identify transplanted human cells that contained host rhodopsin as an indicator of the transplanted RPE cells ability to phagocytose shed photoreceptor outer segments.

Image Acquisition and Analysis

Brightfield images of cresyl violet–stained sections were collected using a DM1000 Leica light microscope and DFC295 Leica camera (Leica Microsystems, Wetzlar Germany). Images were collected from the temporal and nasal region of the retina of each cresyl violet–stained section. Images collected from cresyl violet slides were examined by multiple observers for the location of injection site and suture, ONL thickness, evidence of cells, or untoward pathology. ONL thickness for each section, and maximum ONL thickness for each eye was measured in depth of nuclei.

Confocal z-stack images were acquired from IF-stained sections of retina obtained from all cell-transplanted eyes and from age-matched saline-injected controls using a Leica TCS SP5 compound microscope. A scanning laser confocal microscope (Leica SP5 using LAS AF software; Leica) was used to image stained slides. Laser intensity settings (gain) were kept constant for each emission wavelength (blue 405 nm: 515 V; green 488 nm: 575 V; red 568 nm: 650 V). Z-stack images were collected at ×10 (not shown) and ×20 magnification at 1024 × 1024-resolution with 1-µm step size. Z-stacks were saved as .lif files that contain all image source data. These .lif files were then opened using ImageJ software (http://imagej.nih.gov/ij/; provided in the public domain by the National Institutes of Health, Bethesda, MD, USA). Color channels were kept separate as each color channel z-stack is flattened. Each color channel image was then saved as TIFF files in addition to a color merged image. Cones were quantified by three observers blinded to dosage or age group, with only an animal identifier and the image(s) presented to the observer. Cone counts were then averaged and analyzed.

Repeated measures analysis of variance (ANOVA) with Fisher's post-hoc analysis was used to analyze data. If only two groups were being analyzed, unpaired *t*-tests were performed.

Results

OpRegen Characterization

OpRegen cells used in this study were characterized for identity, purity, potency, and safety (Fig. 1; Table 3). Purity of the cells was tested based on coexpression of CRALBP and PMEL-17 (that, to our knowledge, mark only RPE cells). As shown in Figure 1A, nearly all (99%) of the cells coexpressed CRALBP and PMEL-17 by FACS. Immunostaining of the OpRegen cell culture demonstrated that 95% and 90% expressed Bestrophin 1 and MITF, respectively, by confocal imaging followed by manual counting (Fig. 1B). DNA fingerprinting analysis demonstrated that the identity of OpRegen cells matched with the profile of the source HAD-C 102 hESC line (not shown). To test the potency of the cells, cells were grown in the transwell system. As shown in Figure 1C and summarized in Table 3, OpRegen cells grown for 3 weeks on transwells, demonstrated barrier function (transepithelial electrical resistance; TEER) of 368 Ω and polarized PEDF and VEGF secretion (apical to basal PEDF and basal to apical VEGF ratios were above 1). There was no $Oct4^{+}TRA\text{-}1\text{-}60^{+}$ hESCs impurity in OpRegen cells based on FACS measurement (below the assay limit of detection [LOD] 0.0004%; Fig. 1D) and the karyotype was normal (not shown). The cells were tested sterile in a 14-day bacterial culture

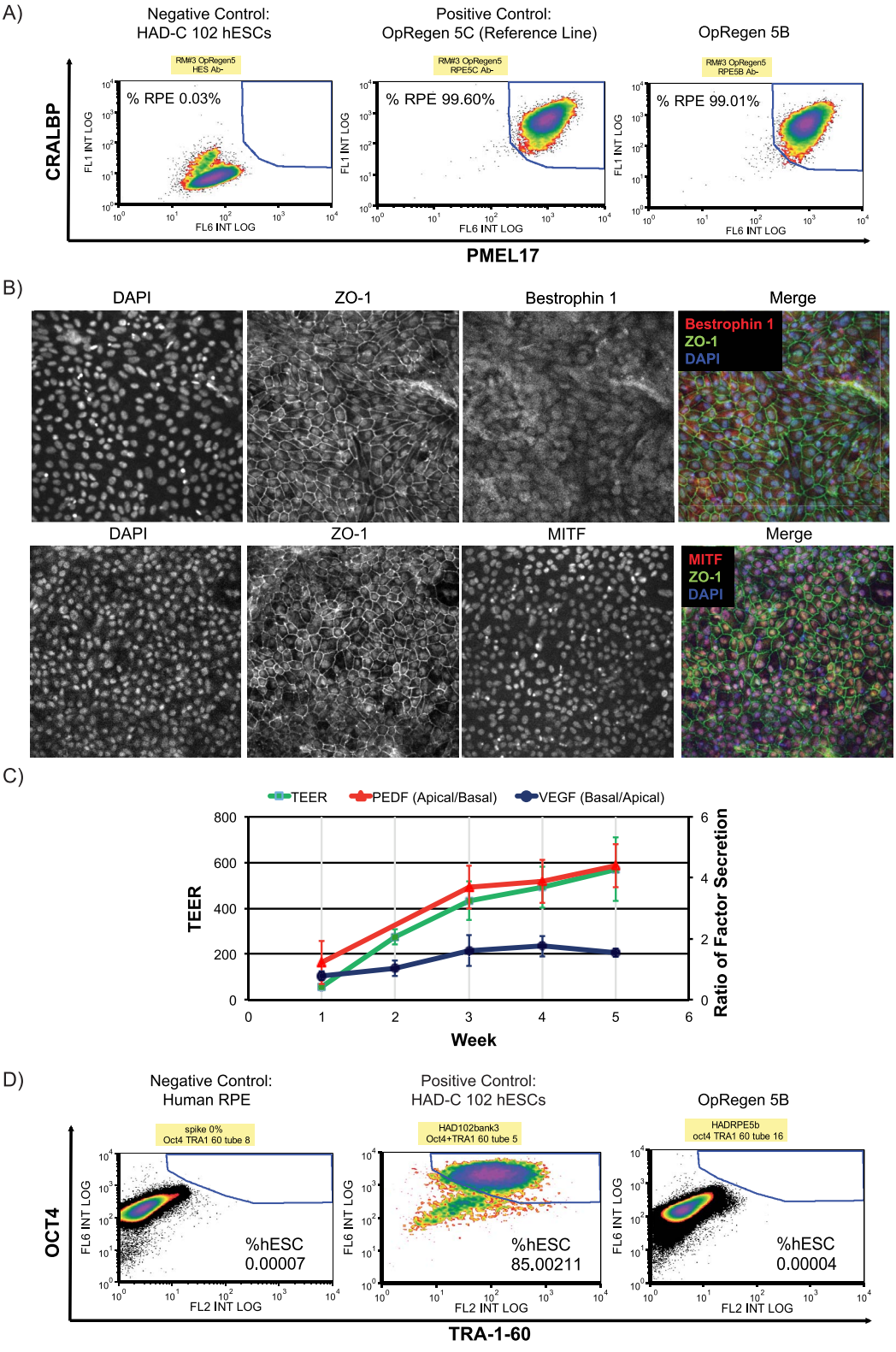

Figure 1. Characterization of OpRegen 5B cells. (A) FACS analysis demonstrating that 99.01% of OpRegen 5B cells coexpress the RPE markers CRALBP and PMEL17. (B) Immunostaining of cultured OpRegen 5B cells followed by confocal imaging and manual counting of 500 DAPI-positive cells using the ImageJ software, demonstrated that 95% of the cells in the culture were positive for Bestrophin 1 and 90% positive for MITF. (C) OpRegen 5B cells cultured on a transwell for 5 weeks demonstrated their ability to generate barrier function →

←
(TEER > 100 Ω) as well as secrete PEDF and VEGF in a polarized manner, PEDF to the apical side (apical to basal PEDF ratio > 1) and VEGF to the basal side (basal to apical VEGF ratio > 1). Data represent average ± standard deviation (SD) of four TEER-, PEDF-, and VEGF-independent measurements of OpRegen five subbatches (5A–5D that were cryopreserved over 4 days). (D) Using a highly sensitive qualified TRA-1-60/Oct4 double staining FACS method (LOD 0.0004%; LOQ [limit of quantification] 0.001%; accuracy and precision ≤ 25%, linearity R2 > 0.99 in the range 0.001%–1%), no hESCs (levels below assay LOD) were detected in OpRegen 5B cells (10×10^6 cells were acquired).

(<USP71>), were mycoplasma-free (<USP63>), and demonstrated endotoxin level (LAL; <USP85>) below 0.03 EU/mL (Table 3).

Functional Outcomes

Post thawing preinjection cell viability for all injection time points averaged 94.0% ± 0.03. Post injection cell viability in the residual injection formulation averaged 92.4% ± 0.02. Color fundus photos collected immediately following injection confirmed successful generation of a subretinal bleb and injection of cells in all animals included in the study; animals without a successful surgery were eliminated from the study. All animals tolerated the anesthesia and injections well and recovered without complication.

OKT thresholds were measured at P60, P100, P150, and P200. OKT thresholds were rescued in all cell-treated groups at all ages (Fig. 2) and these groups outperformed unoperated or BSS+-injected eyes (including contralateral eyes) at all ages. Unoperated control values were similar to those reported previously.[16,24,25,45] There was a significant dose dependent effect between the low dose (25 K) and the two higher doses (100 K [$P < 0.0001$] and 200 K [$P < 0.0001$]), which was most apparent as the animals aged; OKT thresholds following administration of the high dose (200 K) were higher and not significantly different from those obtained with the medium (100 K) dose ($P = 0.5646$). Untreated and

Table 3. A Summary Table Demonstrating Batch Release Testing Results of OpRegen Batch 5B Cells

Test	Acceptance Criteria	OpRegen 5B
Viability (mean ± SD)	≥70%	89% ± 4% ($n = 4$)
Total cells/vial (mean ± SD)	≥0.8×10^6 / Vial	$0.92 \times 10^6 \pm 0.1 \times 10^6$ per vial ($n = 4$)
RPE purity		
% $CRALBP^+PMEL17^+$ RPE Cells	≥ 95%	99.01%
RPE identity		
% Bestrophin 1	≥80%	≥95%
% MITF	≥80%	≥90%
Potency:	For information only	
Barrier function (TEER at week 3)	≥100 Ω	368 Ω
Polarized PEDF secretion (apical/basal ratio at week 3)	>1	3.19
Polarized VEGF Secretion (basal/apical ratio at week 3)	>1	1.91
Safety		
hESC impurity % $Oct4^+TRA\text{-}1\text{-}60^+$ hESCs	<0.01%	<0.00004% (below limit of detection)
Karyotyping	Normal	Normal
Sterility <USP71>	Negative	Negative
Mycoplasma <USP63>	Negative	Negative
Endotoxin	<5EU/mL	0.03 EU/mL

Batch release criteria were defined according to the variability seen in testing different OpRegen batches. The average and SD for viability, total cells/vial, identity, purity and hESCs impurity test results were measured. The criteria for release were measured by subtracting or adding three times the SD from/to, respectively, the average.

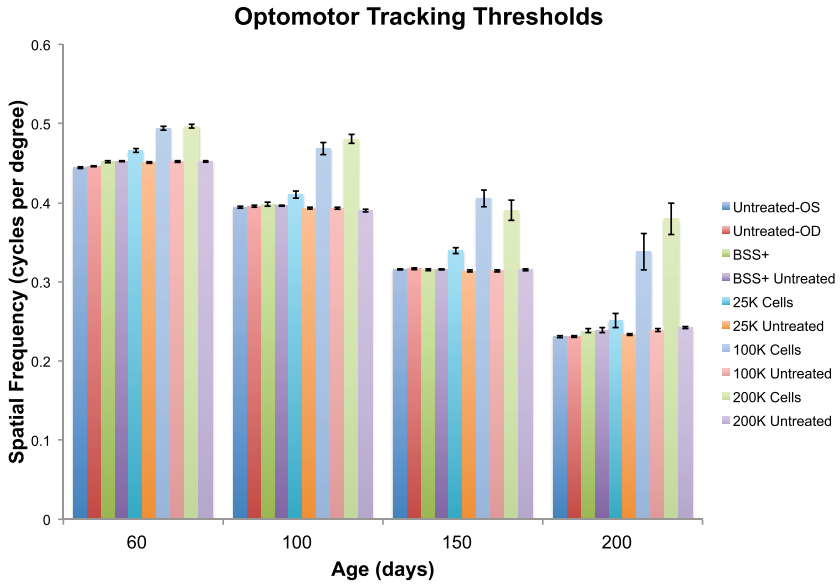

Figure 2. Optokinetic tracking acuity thresholds measured at P60 ($n = 241$), P90 ($n = 178$), P150 ($n = 117$), and P200 ($n = 58$). Cell-treated groups outperformed all controls with the mid (100 K) and high (200 K) dose achieving the best rescue.

BSS+-injected animals' OKT thresholds continued to decline over the course of the study, and did not differ from naïve untreated eyes ($P = 0.6068$) or untreated fellow eyes. In all cell-treated groups, there was rescue of OKT thresholds as compared with the controls, although absolute visual acuity values slowly declined with time in all groups. The decline of OKT thresholds was reduced in the two highest cell doses compared with controls.

Morphological Outcomes

Color fundus photographs were collected from all animals immediately prior to necropsy (Fig. 3). BSS+ and untreated eyes presented with a fundus that appeared normal at 60 days of age, which underwent a darkening discoloration over time with the progressive degeneration of the retina that revealed the underlying choroid. Cell-treated eyes presented with hyper (darker)- and hypo (lighter)-pigmented areas of the retina that corresponded to the location at which cells were deposited in the subretinal space during transplantation (Fig. 3). Such retinal areas with variable pigment levels were not evident in BSS+-injected or unoperated eyes. The distribution of the hyperpigmented areas was often a single large dark area; however, distinguishing this became increasingly difficult as the remainder of the retina darkened with advanced age. The hypopigmented (yellow) spots appeared as bright speckled patterns that were easily visible over the course of the study.

Cresyl violet staining of retinal tissue sections was used to provide metrics of rescue of retinal morphology and to indicate likely areas of grafted cells, which would then be analyzed further using immunohistochemistry. To ensure proper orientation of the eye for histological assessment, and to seal the minor and localized choroidal and scleral damage caused by the surgical approach, a suture was placed at the injection site following transplantation, which was then used as a landmark for the histological study. The injection site, as indicated by the suture material or a small degree of retinal atrophy occasionally occurred at the site of insertion of the injection cannula, was clearly identified in 68 of 159 cell-injected eyes by histology using cresyl violet–stained slides (data not shown). The localized surgical atrophy was always located at the far temporal margin and was characteristic of subretinal injections using the transcleral approach. This small and localized area of damage did not significantly affect visual function as indicated by the BSS+ control group and is often so small it is not detectable using the slide sampling method used in this study.

The percentage of cell-transplanted animals with identified photoreceptor rescue independent of cell dosage was 92% at P60, 90% at P100, 86% at P150, and 18% at P200. We also quantified the maximum rescued ONL thickness represented by the number of rows of photoreceptor nuclei present in each dose group across all sacrifice ages (Fig. 4). In general, maximum photoreceptor protection was observed in

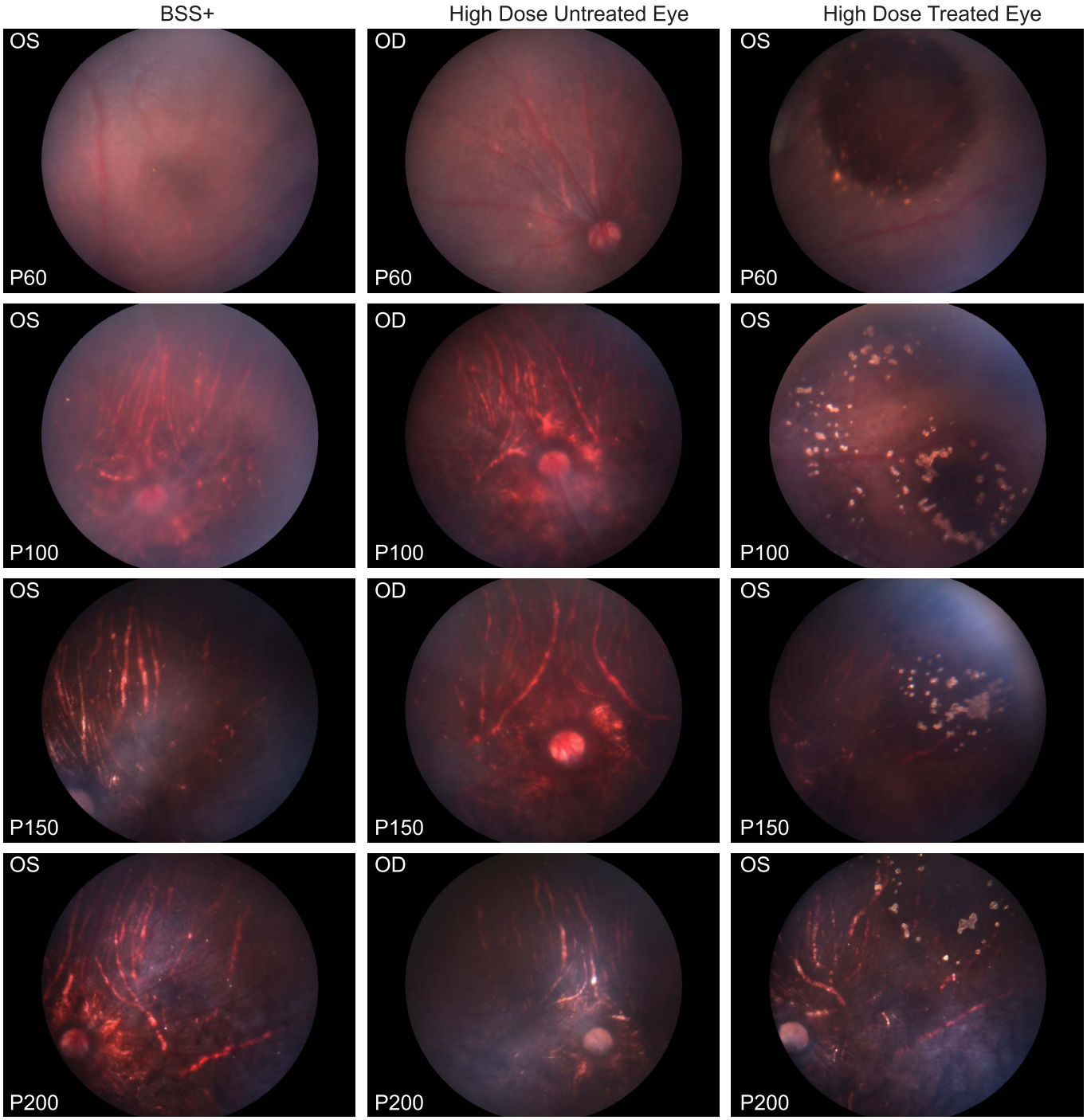

Figure 3. Representative color fundus photographs of vehicle control (BSS+)-injected eyes (OS), high (100 K) dose contralateral untreated eyes (OD), and high dose–treated eyes (OS) immediately prior to sacrifice at age (P) 60, 100, 150, and 200. The hyper- and hypopigmented areas in the high dose–treated eyes (OS) are in the same location as the subretinal blebs were created during surgery (not shown), which indicates that these locations were the location of the transplanted cells.

the slide series adjacent to those that contained the injection site, where transplanted cells were most likely to be present. Cell-treated groups had significantly higher maximum ONL thickness at P60, P100, and P150 (all $P < 0.0001$) than BSS+-treated eyes, however, there was no statistical difference at P200 (Fig. 4). We also quantified the number of cresyl violet–stained slides in which photoreceptor protec-

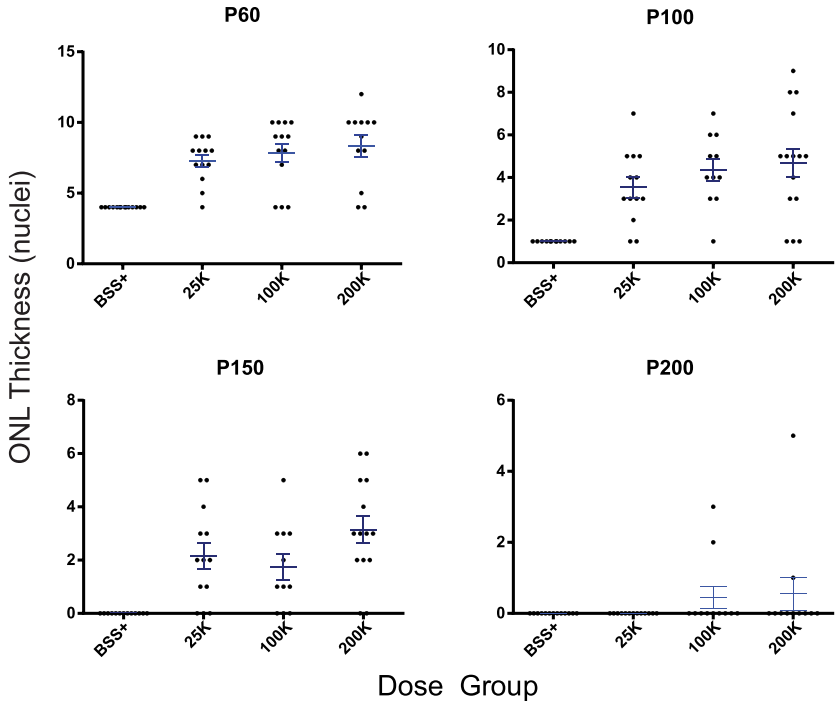

Figure 4. ONL thickness measured in number of nuclei. Each *dot* represents the count of the number of photoreceptor nuclei from each animal from every dose group for all ages. *Panel B* displays the tabularized data of number of slides where ONL thickness was observed above baseline values. Baseline photoreceptor layer thickness of unoperated eyes, equals four (4) at P60, one (1) at P100, and zero (0) at P150 and P200.

tion was observed and plotted those values as a percentage of the total number of slides (data not shown). Because 60 slides were cut from each eye, this percentage is an indication of the size of the rescued area induced in the retina. We found no statistical difference between cell-treated groups until P200, where rescue was no longer observed in the low, 25,000-cell dose. We did observe a decrease in the percentage of slides with observable photoreceptor rescue with age (data not shown).

Representative slides were stained using IF to confirm the presence of transplanted OpRegen cells (Fig. 5, columns 2 and 3). Transplanted cells were positively stained at each survival age using antihuman nuclear marker and antihuman melanoma (PMEL-17) antibodies (Fig. 5, column 2). Transplanted cells were observed always in apposition to a rescued ONL and in the dorsal temporal region of the eye, which corresponded to the location of injection of the cells and the location with the largest areas of photoreceptor rescue (arrows). With increasing age, the number of stained transplanted cells decreased and consequently, the number of rescued photoreceptors also declined, although photoreceptor rescue was consistently higher than baseline levels. In multiple cases, transplanted cells were observed to have integrated into the host RPE cell layer (Figs. 6A–D, Figs. 7A, 7B). A potential mechanism of rescue employed by the transplanted cells is to ingest shed photoreceptor outer segments that constitute the debris zone and removal of the debris zone reduces the toxic and oxidative stress on the photoreceptors, and thus aids in sustaining photoreceptor survival. In all cases where transplanted cells were positively identified, there was an absence of the characteristic RCS debris zone. Therefore, we selected specific animals for evaluation of rhodopsin ingestion by OpRegen, based on positive identification of transplanted cells in retinal sections. In each case tested (n = 6), we observed fluorescently labeled rhodopsin within the transplanted OpRegen cells (representative image in Fig. 6E) indicating that the transplanted RPE cells indeed internalized photoreceptor outer segments.

No tumors or teratomas were observed in any of the eyes. Furthermore, representative sections from each dose group were studied for potential proliferation of transplanted cells. A pellet of OpRegen cells generated from a freshly thawed vial (not shown) and tissue sections from OpRegen-injected eyes (Fig. 5,

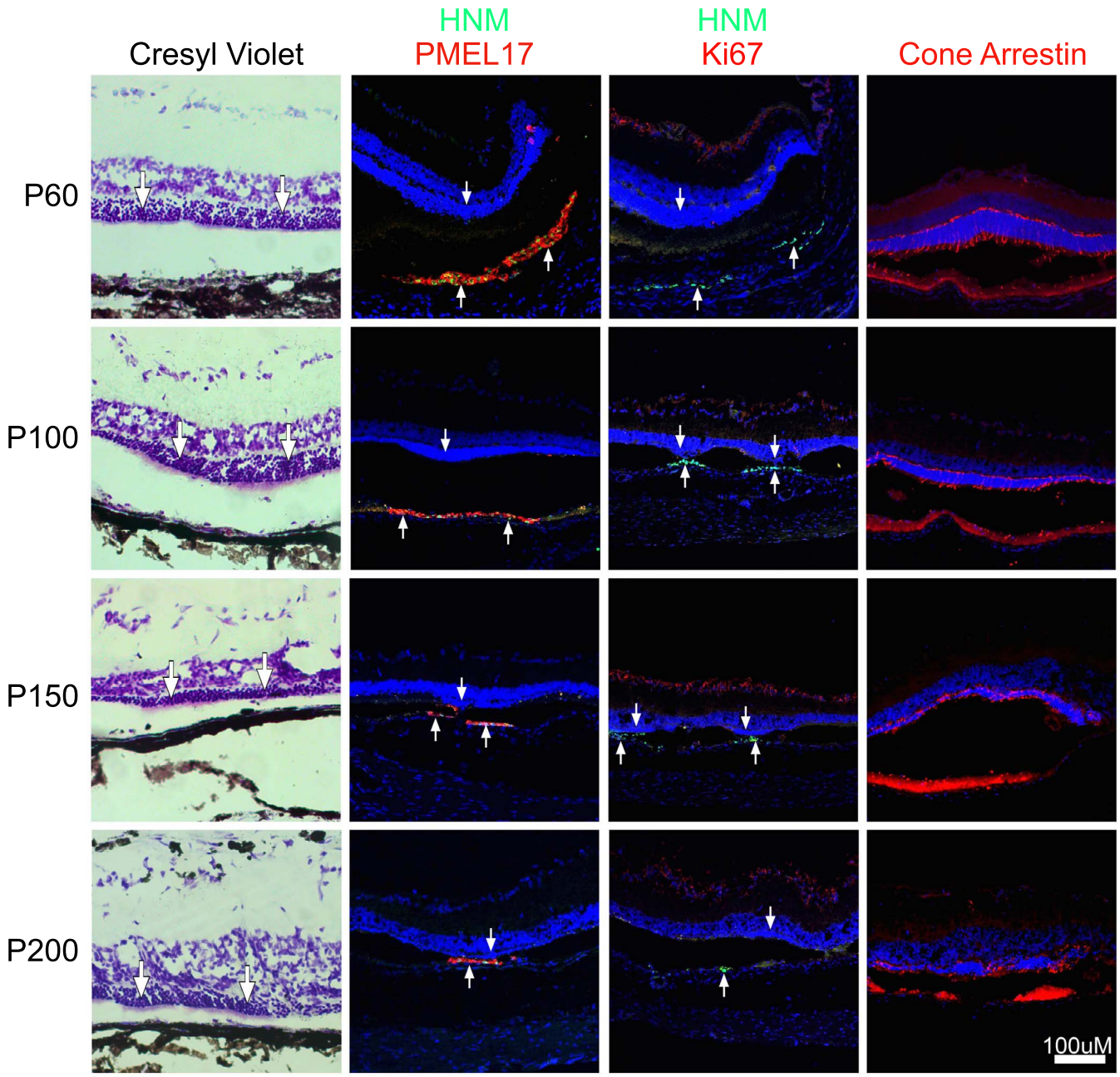

Figure 5. Brightfield and immunofluorescent images of representative experimental cell treated animals at P60, P100, P150, and P200. *Column A* contains images of cresyl violet–stained retina illustrating photoreceptor rescue at each age. *Column B* images illustrate positive survival of transplanted cells as indicated by immunohistochemical staining of human nuclei marker (HNM, *green*), a human RPE marker (antimelanoma gp100/PMEL17, *red*). *Column C* images illustrate the lack of expression of the proliferation marker Ki67 (*red*) in human cells combined with positive human nuclear marker (*green*) at all ages tested. Finally, *column D* images illustrate cone rescue at each age using anti-rat cone arrestin antibody (*red*). DAPI (*blue*) was used for background staining in all immunofluorescent panels to highlight nuclear layers. Human melanoma was used for positive control tissue for PMEL17, human tonsil for Ki67, and juvenile RCS rat retina for cone arrestin (not shown). *Downward arrows* indicate ONL.

column 3) were tested for proliferation using the human specific proliferation marker Ki67 and double stained using antihuman nuclear marker. Human tonsil was also used for positive control tissue. OpRegen cells were negative for Ki67 in both the cell pellet (not shown) and in tissue sections at all ages (Fig. 5, column 3; Figs. 7C, 7D). Thus, OpRegen cells

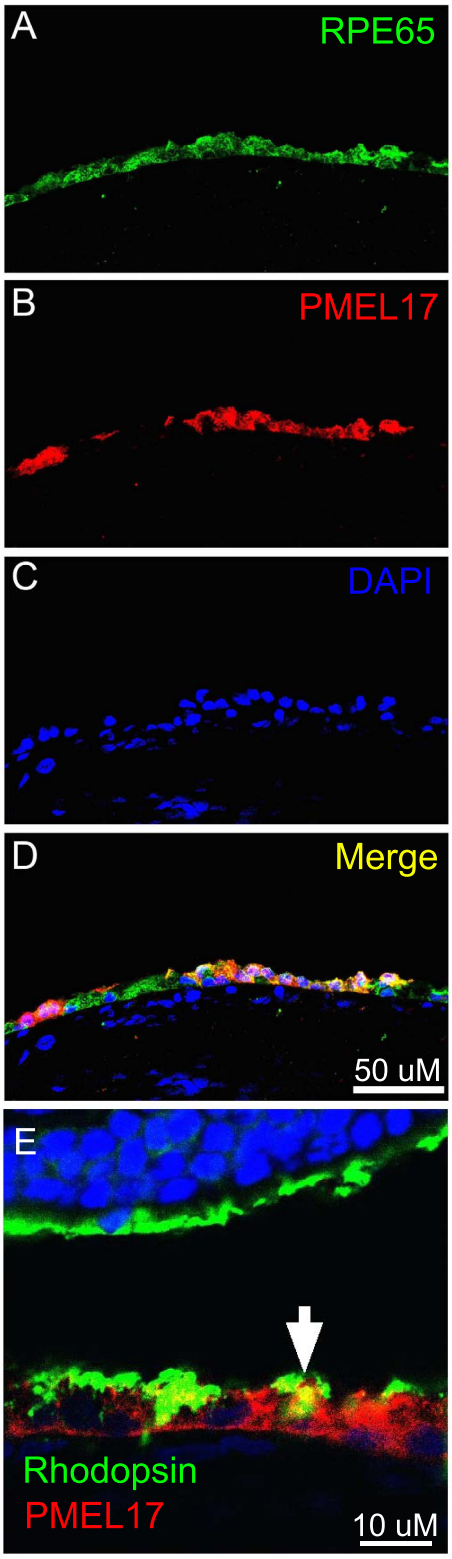

Figure 6. Immunohistochemical analysis of integration of transplanted OpRegen cells into the host rat RPE monolayer. OpRegen were double stained with RPE65 (*Panel A*, which also stains host RPE cells), human specific PMEL17 (*Panel B*), and DAPI (*Panel C*). *Panel D* demonstrates the merged images revealing a combination of human RPE and rat RPE colocalized within an RPE monolayer. *Panel E* illustrates rhodopsin positive tissue within the transplanted cells (*arrows*).

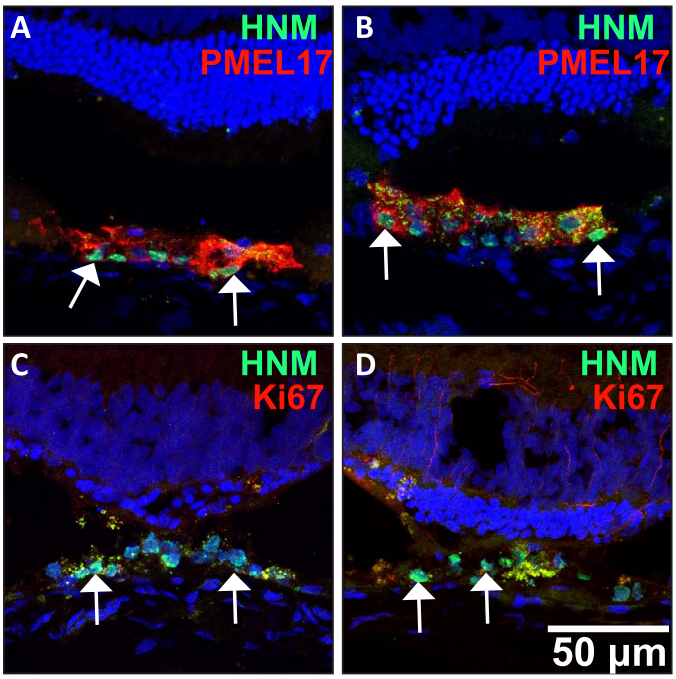

Figure 7. High magnification confocal images of immunohistochemically stained OpRegen at P100 integrated into the host RPE layer. OpRegen stained positively for human nuclear marker (HNM) and human melanasomal protein marker (PMEL17). In addition, transplanted OpRegen did not stain positively for the proliferation marker Ki67 (absence of *red* in [C] and [D]).

were neither proliferating before nor following transplantation.

The behavioral assessment of vision performed in this study was done under photopic conditions that depend predominantly on cone photoreceptor-driven function, and therefore we chose to examine the level of rescue of cone photoreceptors in cell-treated and BSS+-injected eyes. Cone photoreceptors were stained using anticone arrestin antibody that highlights the entire cone profile (Fig. 5, column 4). Cone photoreceptors were quantified from confocal images of tissue sections from cell treated and BSS+-injected eyes collected from sections immediately adjacent to those with maximum ONL thickness. Counts from three observers were averaged and compared between dosage groups and across age. Animals that received cell transplants had significantly higher number of cones than control BSS+-injected eyes at all ages (Fig. 8). Cone photoreceptors

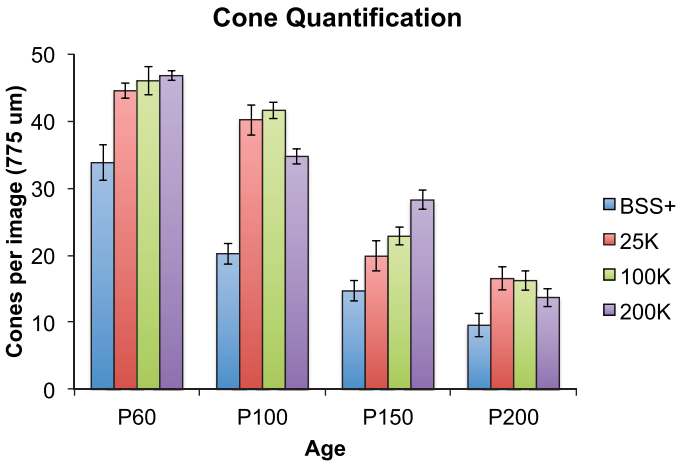

Figure 8. Cone photoreceptor quantification in vehicle control (BSS+; $n = 52$), low dose (25 K cells; $n = 52$)-, middle dose (100 K cells; $n = 46$)-, and high dose (200 K cells; $n = 53$)-treated eyes. Cell-treated eyes had significantly higher numbers of cones compared with vehicle (BSS+) controls at all ages (see text for further details).

at P60 were visibly shorter than at earlier ages or in nondystrophic controls (Fig. 5, column 4).[16] At P100, cones were further reduced in length and by P150 and beyond cones were only recognizable as positively stained nuclei (Fig. 5, column 4). At the later ages (P150 and P200), there were no cones evident in areas of the retina peripheral to the area of rescued retina (data not shown).

Discussion

The results of this study demonstrate that transplantation of OpRegen into the subretinal space of RCS rats protected retinal structure and function long-term. The donor cells attenuated the progressive degeneration of the retina, as reflected in the rescue of behavioral measurements of vision and rod and cone photoreceptor rescue. Transplanted OpRegen cells integrated into the host RPE cell layer and performed the natural physiological function of ingestion of photoreceptor outer segments. This recovery of function resulted in the preservation of rod and cone photoreceptors for up to 180 days post injection. There was no evidence of uncontrolled growth of the transplanted cells and no safety concerns were noted with transplantation of these cells into the subretinal space. Collectively, these data suggest that OpRegen may be a promising therapeutic for the treatment of disorders of the retina that primarily affect the RPE, including AMD and subtypes of retinitis pigmentosa. Indeed, this data combined with data collected in a definitive safety studies (tumorigenicity and spiking and safety/biodistribution) has resulted in an FDA-approved IND (investigational new drug) Phase 1/2a clinical trial for AMD patients (www.clinicaltrials.gov; NCT02286089).

Immune-related rejection of tissue grafts continues to be a concern in cell transplantation therapies. Cell transplantation studies in rodent (including the present study) and primate models have required the use of cyclosporine A or other immune suppressants to suppress T-cell activation, particularly when the graft is xenogeneic in nature.[16,17,46] Following transplantation of OpRegen in the present study, no animals exhibited a rejection of the grafted cells as evidenced by a lack of T or B cells in the subretinal space. We did observe a small number of animals that exhibited signs of inflammation and a mononuclear response localized in the choroid, which is not unexpected given that the surgical approach requires perforation through the choroid and we cannot discount the possibility that some transplanted cells could have leaked into the choroid using this approach. While this immune response would not be unexpected given the xenogeneic nature of the treatment, it should be noted that this response was strictly limited to the choroid and there was no detrimental effect observed on the neural retina due to this inflammatory response. In addition, as this response was limited only to 4 of 53 animals examined, it was more likely caused by improper placement of the cells during the surgical procedure rather than the transplanted cells or the procedure themselves. Based on these results, we expect a similar or better survival of OpRegen in the allogeneic setting under similar immunosuppressive conditions in humans. A confirmatory safety assessment was performed in which an external veterinary ophthalmologist reviewed all cresyl violet–stained slides from the BSS+ and the high cell–dose groups (200 K). No pathological lesions suggestive of hyperplasia or neoplasia were observed. The predominant histopathological finding was minor focal retinal atrophy, associated with focal adhesions to the choroid and sclera. All these lesions are considered related to the procedural administration into the subretinal space via the transcleral route using a fine glass pipette. In addition, 4 of 53 high cell dose–treated animals sacrificed on day 60 of the study, exhibited a change defined as minimal to mild inflammation in the choroid and sclera, but not in

the neural retina or in the vitreous compartment. The inflamed area consisted of mixed mononuclear cell infiltration. It should be noted, however, that even in the few animals with minimal to mild chronic inflammation, the neural retina remained intact and significant photoreceptor preservation was noted.

Functional outcome measurements revealed that vision was significantly preserved in cell-treated eyes compared with controls. The data presented here was recorded from all animals of each group, including those with lower responses (including those with minimal or no OKT rescue), suggesting that the presented data reflects an underestimation of the accurate effect the transplanted cells have on vision rescue (i.e., low-performing animals were included reducing the overall average). OKT values were well maintained until P60 in OpRegen-treated groups but slowly declined thereafter. The decline of OKT was lower in the 100- and 200 K–cell treated groups than in the 25 K and control groups suggesting a strong rescue effect, which was dose dependent. A previous study using hESC-derived RPE cells transplanted into the RCS rat reported rescued OKT thresholds[27]; however, in that report, by approximately P200, animals in some dosage groups no longer responded to the stimulus, and rescued values were significantly lower than those reported here. A potential reason for this difference between these results is that, in the present study, we used higher cell doses (200,000 compared with a max of 100,000) than in the Lu et al.[27] study, which could have resulted in survival of more cells for longer time that translated into continued rescue at a higher level. OpRegen efficacy data demonstrated in this paper is in support with previous studies in RCS rats in which RPE cells derived from hESC and iPSCs were used.[17,26–29,37,47,48] The main difference between OpRegen cells and other hESC- and iPSC-derived RPE cells is the method of differentiation that perhaps will affect the quality of the RPE cell product. Ongoing and future clinical studies will better demonstrate if these differences will be translated into better efficacy outcomes.

Imaging of the retina using color fundus photography immediately post injection was particularly valuable in evaluating the success of the transplantation, including the size and location of the subretinal bleb. This information is particularly helpful for ensuring the proper orientation of the eye prior to embedding in OCT for cryosectioning. Furthermore, fundus photography prior to necropsy provided additional information regarding the cell transplants: the yellow patches in the cell-treated eyes, which are not present in untreated or BSS+–injected eyes, suggest that these locations contained the transplanted cells. We hypothesize that the bright yellow spots are the result of the engrafted cells having ingested a large quantity of shed photoreceptor outer segment debris. This is supported by our findings that these spots are only found in the area of retina where transplanted OpRegen cells were located, and the reduction in yellow spotted areas correlated with a reduction in surviving transplanted cells with age. We confirmed that the transplanted cells contained large amounts of rhodopsin-positive outer segments, and that the outer segment debris zone was absent in the area of the engrafted cells. Despite a similar pattern of cell dispersion previously reported,[42] we cannot definitely state the nature of the yellow deposits.

Transplantation of OpRegen into the RCS rat resulted in significant photoreceptor preservation. Given the nature of retinal rescue induced by RPE cells (specifically phagocytosis) and that the prolonged presence of the transplanted cells is required to maintain prolonged preservation of the retina and vision, we semiqualitatively assessed whether the number of engrafted cells decreased over time (data not shown). We observed a decline in the number of engrafted cells over the course of the study. A number of reasons could account for this decline: first, it is possible that due to the xenogeneic nature of this study, the cells are subject to immune rejection and that incomplete immune suppression would facilitate this process. However, rejection of xenogeneic cells would elicit a strong innate immune response with significant infiltration of mononuclear cells—a response we did not observe in the retina of any animals in this study. An alternative possibility is that transplanted RPE cells are unlikely to survive indefinitely in the subretinal space without integration into the host RPE and adherence to the Bruch's membrane. Finally, we cannot discount the possibility that ingestion of large volumes of shed photoreceptor outer segment debris could impair or perhaps be toxic in some way to the transplanted cells. Evaluation of this properly, well-controlled in vitro study, would need to be performed from live RPE cells recovered from the subretinal space at specific time intervals following transplantation. While particularly intriguing, these studies would be very difficult, have not yet been performed, and were beyond the scope of the present study. However, despite a decline in the number of surviving transplanted cells over time in the present study, which has also been documented in

one form or another in other RPE cell transplantation studies,[27,28] the rescue effect the transplanted cells exert on the host retina and visual function was extended long-term.

Transplanted OpRegen appeared to integrate into the host RPE cell layer in some, but not all animals. Recent literature suggests the possibility of transfer of cytoplasmic and perhaps genetic material from the transplanted cells into host cells.[49,50] In each of these published studies, transplantation of photoreceptors, or photoreceptor precursor cells, have been demonstrated to transfer material to host photoreceptor cells, although the authors describe that no nuclear fusion had occurred. In the present study, we observe antihuman nuclear marker–positive RPE cells integrated into the host RPE cell layer (Figs. 5 and 6). While it is possible that other human proteins that we stained for in this study could be transferred to host (rodent) RPE cells, such as RPE65 and or PMEL17, we only observed these markers in cells that also contained a nucleus that stained positively for human nuclear marker, and therefore, we conclude that material transfer between transplanted and host cells was unlikely in this study.

Quantification of cone photoreceptors, which were easily identified using an anticone arrestin antibody, revealed a significant preservation of cones in cell-treated eyes compared with controls, however, there was no significant difference within the cell-treated groups, which closely resembles the outcomes from measurements of visual function (Fig. 7), and closely resembles cone preservation previously reported.[16] The location of cone cell rescue was limited to the dorsal temporal region of the eye, which corresponds to the location of the transplanted RPE cells. Because cone photoreceptors and their function subserve the visual function measured in the OKT system and because cones will be the primary target for rescue in human conditions, we hypothesize that OpRegen is likely to incur the same beneficial effect in the cone function dominant human macula. While cone photoreceptors and cone function was rescued as described above, preservation of the ONL observed in this study suggests the rescued of rod photoreceptors as well. Therefore, OpRegen has the capacity to rescue both photoreceptor types that are present in the human retina, including the macula.

In summary, upon transplantation into the subretinal space of RCS rats, OpRegen cells are safe and provide a significant benefit to the degenerating retina. Based on the results reported here, and a long-term safety study in NOD/SCID mice (unpublished), OpRegen cells appear to meet the necessary criteria for translation into use for the treatment of human retinal degenerative diseases. Indeed, a Phase 1/2a clinical trial for transplanting OpRegen in patients with advanced dry AMD and GA is currently ongoing.

Acknowledgements

The authors thank Miri Gov, Ohad Cohen, Alex Obolensky, Bat Shachaf, Shosh Merchav, and Abraham Nyska for their scientific support.

Supported by grants from Cell Cure Neurosciences, Unrestricted departmental funding from Research to Prevent Blindness (New York, NY), departmental core grant P30 EY010572 from the National Institutes of Health (Bethesda, MD).

Disclosure: **T.J. McGill,** (F); **O. Bohana-Kashtan,** (E); **J.W. Stoddard,** None; **M.D. Andrews,** None; **N. Pandit,** None; **L.A. Rosenberg-Belmaker,** (E); **O. Wiser,** (E); **L. Matzrafi,** (E); **E. Banin,** (C), (P); **B. Reubinoff,** (I); **N. Netzer,** (E); **C. Irving,** (E)

References

1. Friedman DS, O'colmain BJ, Munoz B, et al. Prevalence of age-related macular degeneration in the United States. *Arch Ophthalmol*. 2004;122: 564–572.
2. National Eye Institute. Age-related macular degeneration (AMD). National Institutes of Health, Bethesda, MD. Available at: https://www.nei.nih.gov/eyedata/amd. Accessed January 2012; cited January 5, 2017.
3. Klein R, Klein BE, Linton KL. Prevalence of age-related maculopathy. The Beaver Dam Eye Study. *Ophthalmology*. 1992;99:933–943.
4. Varma R, Fraser-Bell S, Tan S, Klein R, Azen SP; for the Los Angeles Latino Eye Study Group. Prevalence of age-related macular degeneration in Latinos: the Los Angeles Latino eye study. *Ophthalmology*. 2004;111:1288–1297.
5. AREDS Research Group. A randomized, placebo-controlled, clinical trial of high-dose supplementation with vitamins C and E, beta carotene, and zinc for age-related macular degeneration and vision loss: AREDS report no. 8. *Arch Ophthalmol*. 2001;119:1417–1436.

6. AREDS Research Group. Secondary analyses of the effects of lutein/zeaxanthin on age-related macular degeneration progression: AREDS2 report No. 3. *JAMA Ophthalmol*. 2014;132:142–149.
7. Guerin K, Gregory-Evans CY, Hodges MD, et al. Systemic aminoglycoside treatment in rodent models of retinitis pigmentosa. *Exp Eye Res*. 2008;87:197–207.
8. Duncan JL, Paskowitz DM, Nune GC, et al. Retinal damage caused by photodynamic therapy can be reduced using BDNF. *Adv Exp Med Biol*. 2006;572:297–302.
9. Lavail MM, Yasumura D, Matthes MT, et al. Protection of mouse photoreceptors by survival factors in retinal degenerations. *Invest Ophthalmol Vis Sci*. 1998;39:592–602.
10. Lawrence JM, Keegan DJ, Muir EM, et al. Transplantation of Schwann cell line clones secreting GDNF or BDNF into the retinas of dystrophic Royal College of Surgeons rats. *Invest Ophthalmol Vis Sci*. 2004;45:267–274.
11. Faktorovich EG, Steinberg RH, Yasumura D, Matthes MT, Lavail MM. Photoreceptor degeneration in inherited retinal dystrophy delayed by basic fibroblast growth factor. *Nature*. 1990:347:83–86.
12. Faktorovich EG, Steinberg RH, Yasumura D, Matthes MT, Lavail MM. Basic fibroblast growth factor and local injury protect photoreceptors from light damage in the rat. *J Neurosci*. 1992;12:3554–3567.
13. Lavail MM, Faktorovich EG, Hepler JM, et al. Basic fibroblast growth factor protects photoreceptors from light-induced degeneration in albino rats. *Ann N Y Acad Sci*. 1991;638:341–347.
14. Lavail MM, Matthes MT, Yasumura D, Faktorovich EG, Steinberg RH. Histological method to assess photoreceptor light damage and protection by survival factors. In: Lavail MM, Hollyfield JG, Anderson RE, eds. *Degenerative Retinal Diseases*. New York, NY: Plenum Press; 1997:369–384.
15. Lu B, Wang S, Girman S, Mcgill T, Ragaglia V, Lund R. Human adult bone marrow-derived somatic cells rescue vision in a rodent model of retinal degeneration. *Exp Eye Res*. 2010;91:449–455.
16. Mcgill TJ, Cottam B, Lu B, et al. Transplantation of human central nervous system stem cells - neuroprotection in retinal degeneration. *Eur J Neurosci*. 2012;35:468–477.
17. Mcgill TJ, Lund RD, Douglas RM, Wang S, Lu B, Prusky GT. Preservation of vision following cell-based therapies in a model of retinal degenerative disease. *Vision Res*. 2004;44:2559–2566.
18. Forest DL, Johnson LV, Clegg DO. Cellular models and therapies for age-related macular degeneration. *Dis Model Mech*. 2015;8:421–427.
19. Schwartz SD, Hubschman JP, Heilwell G, et al. Embryonic stem cell trials for macular degeneration: a preliminary report. *Lancet*. 2012;379:713–720.
20. Schwartz SD, Regillo CD, Lam BL, et al. Human embryonic stem cell-derived retinal pigment epithelium in patients with age-related macular degeneration and Stargardt's macular dystrophy: follow-up of two open-label phase 1/2 studies. *Lancet*. 2015;385:509–516.
21. D'cruz PM, Yasumura D, Weir J, et al. Mutation of the receptor tyrosine kinase gene Mertk in the retinal dystrophic RCS rat. *Hum Mol Genet*. 2000;9:645–651.
22. Lavail MM, Mullen RJ. Role of the pigment epithelium in inherited retinal degeneration analyzed with experimental mouse chimeras. *Exp Eye Res*. 1976;23:227–245.
23. Lavail MM, Sidman RL, Gerhardt CO. Congenic strains of RCS rats with inherited retinal dystrophy. *J Hered*. 1975;66:242–244.
24. Mcgill TJ, Lund RD, Douglas RM, et al. Syngeneic Schwann cell transplantation preserves vision in RCS rat without immunosuppression. *Invest Ophthalmol Vis Sci*. 2007;48:1906–1912.
25. Mcgill TJ, Douglas RM, Lund RD, Prusky GT. Quantification of spatial vision in the Royal College of Surgeons rat. *Invest Ophthalmol Vis Sci*. 2004;45:932–936.
26. Lund RD, Wang S, Klimanskaya I, et al. Human embryonic stem cell-derived cells rescue visual function in dystrophic RCS rats. *Cloning Stem Cells*. 2006;8:189–199.
27. Lu B, Malcuit C, Wang S, et al. Long-term safety and function of RPE from human embryonic stem cells in preclinical models of macular degeneration. *Stem Cells*. 2009;27:2126–2135.
28. Carr AJ, Vugler AA, Hikita ST, et al. Protective effects of human iPS-derived retinal pigment epithelium cell transplantation in the retinal dystrophic rat. *PLoS One*. 2009;4:e8152.
29. Coffey PJ, Girman S, Wang SM, et al. Long-term preservation of cortically dependent visual function in RCS rats by transplantation. *Nat Neurosci*. 2002;5:53–56.
30. Durlu YK, Tamai M. Transplantation of retinal pigment epithelium using viable cryopreserved cells. *Cell Transplant*. 1997;6:149–162.

31. Gias C, Jones M, Keegan D, et al. Preservation of visual cortical function following retinal pigment epithelium transplantation in the RCS rat using optical imaging techniques. *Eur J Neurosci*. 2007; 25:1940–1948.
32. Girman SV, Wang S, Lund RD. Cortical visual functions can be preserved by subretinal RPE cell grafting in RCS rats. *Vision Res*. 2003;43:1817–1827.
33. Grisanti S, Szurman P, Jordan J, Kociok N, Bartz-Schmidt KU, Heimann K. Xenotransplantation of retinal pigment epithelial cells into RCS rats. *Jap J Ophthalmol*. 2002;46:36–44.
34. Lavail MM, Li L, Turner J, Yasumura D. Retinal pigment epithelial cell transplantation in RCS rats: normal metabolism in rescued photoreceptors. *Exp Eye Res*. 1992;55:555–562.
35. Li LX, Sheedlo HJ, Turner JE. Long-term rescue of photoreceptor cells in the retinas of RCS dystrophic rats by RPE transplants. *Prog Brain Res*. 1990;82:179–185.
36. Pinilla I, Cuenca N, Sauve Y, Wang S, Lund RD. Preservation of outer retina and its synaptic connectivity following subretinal injections of human RPE cells in the Royal College of Surgeons rat. *Exp Eye Res*. 2007;85:381–392.
37. Sauve Y, Girman SV, Wang S, Keegan DJ, Lund RD. Preservation of visual responsiveness in the superior colliculus of RCS rats after retinal pigment epithelium cell transplantation. *Neuroscience*. 2002;114:389–401.
38. Sheedlo HJ, Li L, Barnstable CJ, Turner JE. Synaptic and photoreceptor components in retinal pigment epithelial cell transplanted retinas of Royal College of Surgeons dystrophic rats. *J Neurosci Res*. 1993;36:423–431.
39. Wang S, Lu B, Girman S, Holmes T, Bischoff N, Lund RD. Morphological and functional rescue in RCS rats after RPE cell line transplantation at a later stage of degeneration. *Invest Ophthalmol Vis Sci*. 2008;49:416–421.
40. Cyranoski D. Japanese woman is first recipient of next-generation stem cells. *Nature News*. 2014; September 12.
41. Tannenbaum SE, Turetsky TT, Singer O, et al. Derivation of xeno-free and GMP-grade human embryonic stem cells–platforms for future clinical applications. *PLoS One*. 2012;7:e35325.
42. Idelson M, Alper R, Obolensky A, et al. Directed differentiation of human embryonic stem cells into functional retinal pigment epithelium cells. *Cell Stem Cell*. 2009;5:396–408.
43. Douglas RM, Alam NM, Silver BD, Mcgill TJ, Tschetter WW, Prusky GT. Independent visual threshold measurements in the two eyes of freely moving rats and mice using a virtual-reality optokinetic system. *Vis Neurosci*. 2005;22:677–684.
44. Prusky GT, Alam NM, Beekman S, Douglas RM. Rapid quantification of adult and developing mouse spatial vision using a virtual optomotor system. *Invest Ophthalmol Vis Sci*. 2004;45: 4611–4616.
45. Mcgill TJ, Prusky GT, Douglas RM, et al. Discordant anatomical, electrophysiological, and visual behavioral profiles of retinal degeneration in rat models of retinal degenerative disease. *Invest Ophthalmol Vis Sci*. 2012;53:6232–6244.
46. Francis PJ, Wang S, Zhang Y, et al. Subretinal transplantation of forebrain progenitor cells in nonhuman primates: survival and intact retinal function. *Invest Ophthalmol Vis Sci*. 2009;50: 3425–3431.
47. Thomas BB, Zhu D, Zhang L, et al. Survival and functionality of hESC-derived retinal pigment epithelium cells cultured as a monolayer on polymer substrates transplanted in RCS rats. *Invest Ophthalmol Vis Sci*. 2016;57:2877–2887.
48. Kamao H, Mandai M, Okamoto S, et al. Characterization of human induced pluripotent stem cell-derived retinal pigment epithelium cell sheets aiming for clinical application. *Stem Cell Reports*. 2014;2:205–218.
49. Singh MS, Balmer J, Barnard AR, et al. Transplanted photoreceptor precursors transfer proteins to host photoreceptors by a mechanism of cytoplasmic fusion. *Nat Commun*. 2016;7: 13537.
50. Pearson RA, Gonzalez-Cordero A, West EL, et al. Donor and host photoreceptors engage in material transfer following transplantation of post-mitotic photoreceptor precursors. *Nat Commun*. 2016;7:13029.